Geophysical Research Letters

Supporting Information for

Impact of increasing heatwaves on U.S. ozone episodes in the 2050s: Results from a multi-model analysis using extreme value theory

L. Shen[1], L. J. Mickley[1] and E. Gilleland[2]

[1] School of Engineering and Applied Sciences, Harvard University, Cambridge, Massachusetts, USA
[2] Research Applications Laboratory, National Center for Atmospheric Research, Boulder, Colorado, USA

Contents of this file

Introduction

This supplementary material provides further details of the method and data used in this work. Text S1 describes tests of the methods and datasets used to identify observed ozone suppression. Text S2 describes the test of ozone suppression in GEOS-Chem. Text S3 introduces the point process model in extreme value theory. Text S4 supplies details about the calculation of the standard deviation of projected ozone episodes in the future climate. Figures S1-S9 support the conclusions of this work; more details on these figures can be found in the main text. Table S1 lists all the downscaled climate models used in this study.

Text S1. Test of methods and datasets used to identify ozone suppression

We test the robustness of our approach to identify ozone suppression by comparing the spatial distributions of this phenomenon calculated using different temperature datasets and different preprocessing methods. In Section 2, we use daily maximum temperatures (*Tmax*) from the North America Regional Reanalysis (NARR). As a first test, we detrend the observed maximum daily 8-hour average (MDA8) ozone concentrations by first subtracting the 2003-2012 linear trend from the raw data, and then adjusting the ozone distribution in 2003-2007 to match that in 2008-2012. We adjust the distribution using Quantile Mapping, as in *Gudmundsson et al.* [2012]. Figure S1a shows the resulting spatial distribution of observed ozone suppression, calculated with daily *Tmax* from NARR for May-September from 2003 to 2012. Figure S1b shows the spatial distribution of ozone suppression calculated with daily *Tmax* from the statistically downscaled gridded dataset (1/8°×1/8°) by *Maurer et al.* [2002]. This gridded dataset extends from 2003 only until 2010, and was also used in *Steiner et al.* [2010]. For Figure S1c, we diagnose ozone suppression using *Tmax* values provided by Global Surface Summary of the Day (GSOD). Finally, Figure S1d shows ozone suppression calculated with the NARR daily mean temperatures instead of daily *Tmax*. All results identify a similar spatial pattern of ozone suppression as in Figure 1, suggesting that ozone suppression is a widespread phenomenon in the Northeast, Midwest, Southwest, and a few sites in the deep South. We also test a series of different boundary temperatures between the normal (30^{th}-70^{th} percentiles) and high (90^{th}-97.5^{th} percentiles) temperature regimes over the 816 sites in this study. The distributions of EPA sites in our tests showing ozone suppression are similar to those in Figures 1 and S1. We find that the number of sites exhibiting ozone suppression ranges from 150 to 164 (~20%). Of those sites showing ozone suppression, only 6-40 sites show positive $dO_3/Tmax$ slopes and 0-3 sites show significantly positive slopes above the cut-off temperature.

Text S2. Test of ozone suppression in GEOS-Chem

To investigate the causes of ozone suppression, we perform sensitivity simulations with GEOS-Chem, a chemical transport model that has been used extensively to study ozone air quality in the United States [e.g., *Zhang et al.,* 2014; *Mao et al.,* 2013]. Here we apply version 10-01 (http://geos-chem.org/) with updated ozone-isoprene chemistry [*Paulot et al.,* 2009a; 2009b], driven by GEOS5 assimilated meteorological data from the NASA Global Modeling and Assimilation System (GMAO) for 2004-2012. The model has a horizontal resolution of 0.5°×0.667° with 47 pressure levels over North America (140-40°W, 10-70°N), nested within a global simulation with horizontal resolution of 4°×5°. Biogenic emissions are from the inventory of *Guenther et al.* [2012]. We follow *Hudman et al.* [2012] for emissions of nitrogen oxides (NOx) from soil, and *Murray et al.* [2012] for lightning NOx. U.S. anthropogenic emissions are from the EPA National Emissions Inventory (NEI). To correct the overestimate of mobile NOx emissions in the NEI inventory reported in previous studies [*Yu et al.,* 2012; *Goldberg et al.,* 2014; *Anderson et al.,* 2014; *Canty et al.,* 2015] and to reduce the bias between simulated and observed ozone, we prescribe a 50% decrease of mobile NOx emission in the United States as in *Travis et al.* [2015].

Text S3. Extreme value model

We model the daily MDA8 ozone concentrations conditionally on daily maximum temperature (*Tmax),* using a non-stationary PP model, which formulates the Poison process limit of extreme ozone concentrations above a threshold [*Coles,* 2001; *Rieder et al.,* 2013]. Too low a threshold leads to a bias in the model parameters, while too high a threshold reduces the number of datapoints to constrain the model and increases uncertainty in these parameter estimates. Following *Rieder et al.* [2010], we use the 90th percentile value of ozone concentrations at each site as the model threshold (denoted as u in the equations below) for that site. Let $\{y_t\}$ be the observed daily MDA8 ozone concentrations with associated covariates of daily maximum temperature $\{T_t\}$. Following PP model theory as in *Coles* [2001], the MDA8 ozone concentrations above the 90th percentile for each site, conditioned on a specific temperature *Tmax* and time *t,* can then be expressed as a marginal distribution:

$$p(y_t \geq y \mid t,T) = \frac{1}{n_a}[1+\xi(\frac{y-\mu_{t,T}}{\phi_T})]^{-1/\xi} \quad (E10)$$

where y_t is the daily observed MDA8 ozone from each individual AQS site, n_a is the number of observations in each year, $\mu_{t,T}$ is the location parameter conditioned on both time t (e.g., 2003, 2004, etc.) and daily maximum temperature T, ϕ_T (> 0) is the scale parameter conditioned on *Tmax*, ξ is the shape factor, and f and g are linear functions. The value of n_a is 153, the total number of days from May 1 to September 30. The scale parameter controls the spread of the distribution, while the shape parameter determines the shape of the tails. More details on the PP model can be found in *Coles* [2001]. The expected probability of daily MDA8 ozone exceeding the national air quality standard (NAAQS, 75 ppbv), conditioned on a specific temperature *Tmax* and time *t*, is thus calculated as

$$p(y_t \geq 75 \mid t,T) = \frac{1}{n_a}[1+\hat{\xi}(\frac{75-\hat{\mu}_{t,T}}{\hat{\phi}_{t,T}})]^{-1/\hat{\xi}} \quad (E11)$$

To justify inclusion of temperature in our extreme value theory (EVT) model for maximum daily 8-hour average (MDA8) ozone, we apply the likelihood ratio test to observations at each site. We use the *extRemes* software package [*Gilleland et al.,* 2011]. The base model is a stationary point process (PP) model with no covariates. The test model is a non-stationary PP model, with the scale factor a function of maximum daily temperature (*Tmax*). Suppose the negative log-likelihood is x for the base model and y for the test model. The likelihood-ratio statistic $D=-2*(y-x)$ then follows the chi-square distribution [*Coles,* 2001; *Reiss and Thomas*, 2007; *Gilleland et al.,* 2011]. We find 11.7% of the sites do not show significantly improved performance if we include daily *Tmax* as a covariate in the model. These sites are mainly located to the south of 35°N, where the correlation coefficients r of daily MDA8 ozone and daily *Tmax* range between -0.2 and 0.2 (Figure S3b-c). Following Reiss and Thomas [2007], we also test if the ozone depends on temperature in the tails. We find that sites showing no tail dependence

are located in the south (Figure S3d), consistent with the likelihood ratio test. Our results suggest that increases in surface temperature will have negligible effect on ozone episodes at these sites, and we do not project the future changes in episode number there.

Text S4. Standard deviation of the simulated changes in ozone episode days

We write the external and internal standard deviations of changes in ozone episode days calculated from the 19 projections in different CMIP5 models over all bootstrap simulations as below.

$$\sigma_{internal} = \frac{\sum_{i=1}^{19} \sqrt{\sum_{j=1}^{n} (\Delta x_{i,j} - \overline{\Delta x_i})^2 / n}}{19} \qquad (E12)$$

$$\sigma_{external} = \sqrt{\frac{\sum_{i=1}^{19} \left(\overline{\Delta x_i} - \overline{\Delta x}\right)^2}{19}} \qquad (E13)$$

$$\overline{\Delta x_i} = \frac{\sum_{j=1}^{n} \Delta x_{i,j}}{n} \qquad (E14)$$

where $\Delta x_{i,j}$ is the changes in ozone episode days by 2050s in the i^{th} ($1 \le i \le 19$) model and j^{th} ($1 \le j \le n$) bootstrap simulations, $\overline{\Delta x_i}$ is the average change across all bootstrap simulations in the i^{th} ($1 \le i \le 19$) model, $\sigma_{internal}$ is the standard deviation caused by the "internal" uncertainty of the parameters in the hybrid-EVT model, and the $\sigma_{external}$ is the standard deviation caused by the "external" uncertainty in the different temperature projections across the 19 CMIP5 models.

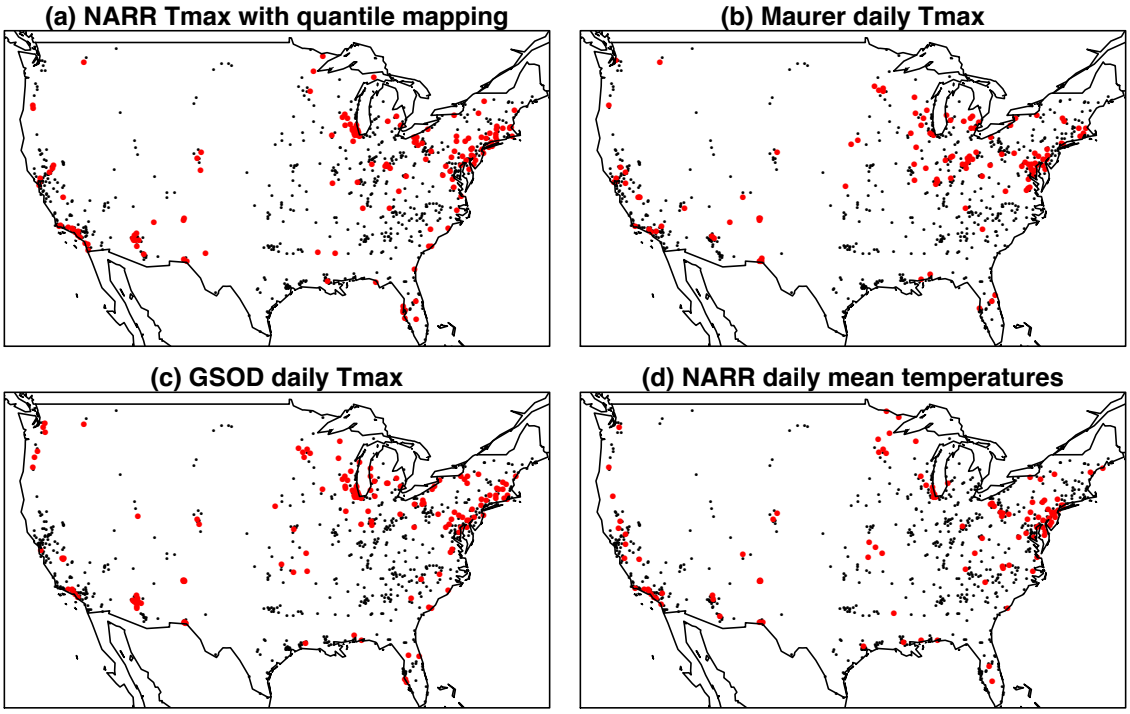

Figure S1. Distribution of EPA-AQS sites exhibiting "ozone suppression" at high temperatures, calculated using different datasets and preprocessing methods. We define ozone suppression as a statistically significant decrease in the slope of daily MDA8 ozone vs. daily *Tmax* occurring above the 95th percentile in *Tmax*. The panels show ozone suppression calculated using (a) 2003-2012 *Tmax* from NARR, (b) statistically downscaled *Tmax* from Maurer et al. [2002] for 2003-2012, (c) 2003-2012 observations of *Tmax* from GSOD, and (d) 2003-2012 daily mean temperatures from NARR. Panel (a) uses detrended ozone concentrations; Panels (b-d) use the original ozone data (i.e., not detrended). See text for more details.

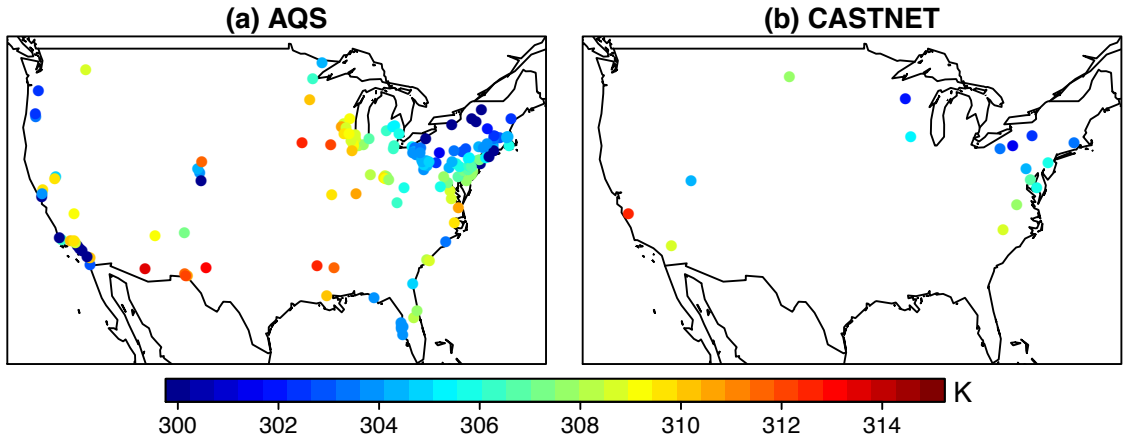

Figure S2. Map of daily maximum cut-off temperatures, above which ozone suppression occurs for (a) AQS and (b) CASTNET sites. Only those sites exhibiting ozone suppression at high temperatures are shown. See text for definition of ozone suppression.

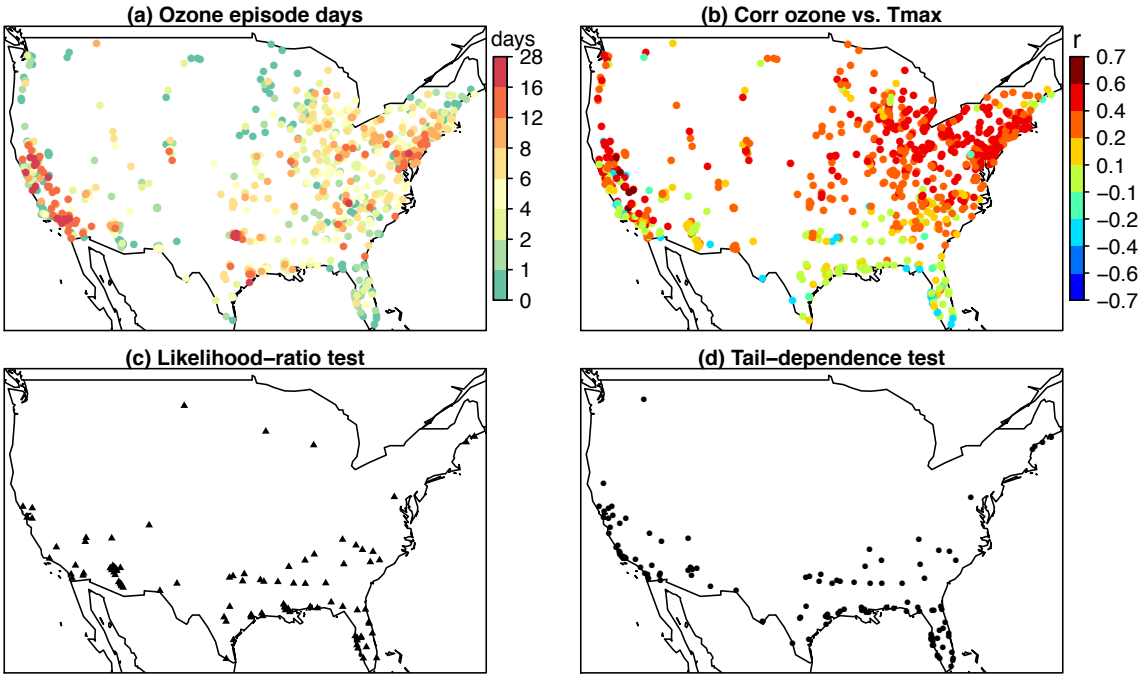

Figure S3. (a) The annual mean number of observed ozone episodes for May-September from 2003 to 2012. Ozone episode days are defined as days with MDA8 ozone above 75 ppbv. (b) The correlation coefficient *r* of daily MDA8 ozone concentrations and daily maximum temperatures (*Tmax*) in May-September during 2003-2012. (c) The sites where the inclusion of *Tmax* does not improve the EVT model for daily MDA8 ozone. (d) The sites where the daily MDA8 ozone show no tail dependence on *Tmax*.

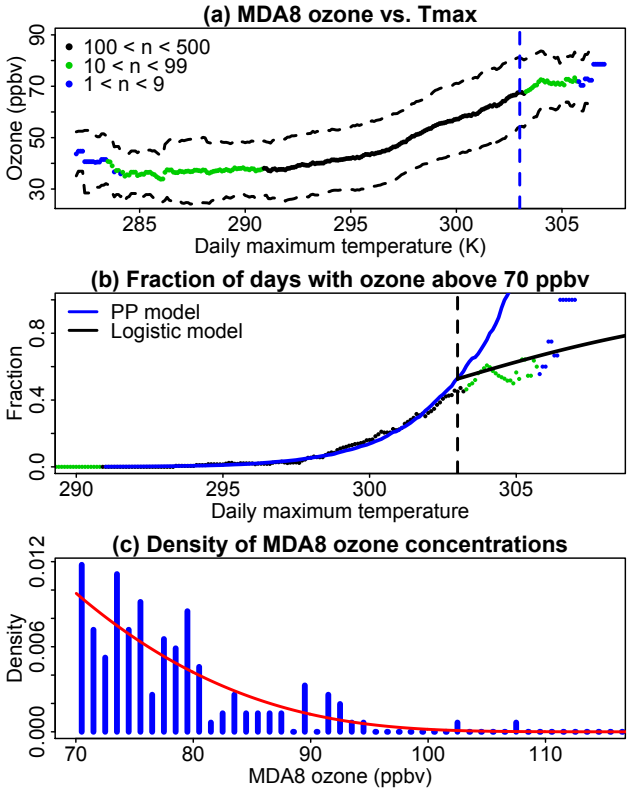

Figure S4. (a) Daily MDA8 ozone concentrations as a function of daily maximum temperatures (*Tmax*) at a sample EPA-AQS site (76.0W, 41.2N) in Nanticoke, PA, during May-September from 2003 to 2012. The color points denote the MDA8 ozone concentrations averaged in a 2-K-wide moving temperature window. Different colors represent the number of points in each 2-K bin, and the dashed lines show the confidence interval with one standard deviation. The cut-off temperature at which we detect a significant change in the ozone-T slope is shown as the blue dashed line at 303 K. (b) Fraction of MDA8 ozone above the EVT model threshold (70 ppbv) as a function of *Tmax* (Equation E5). The fitted fraction for temperatures below 303 K, as denoted as the blue curve, is calculated using a point process model. The fitted fraction with temperatures above 303 K (black line) is calculated by logistic regression. The observed ozone fraction within each 2-K window is shown by colored points as in Panel (a). (c) Observed (blue bars) and simulated (solid black line) distribution of extreme ozone concentrations above 70 ppb. The simulated distribution is calculated using the hybrid extreme value model, as described in the text.

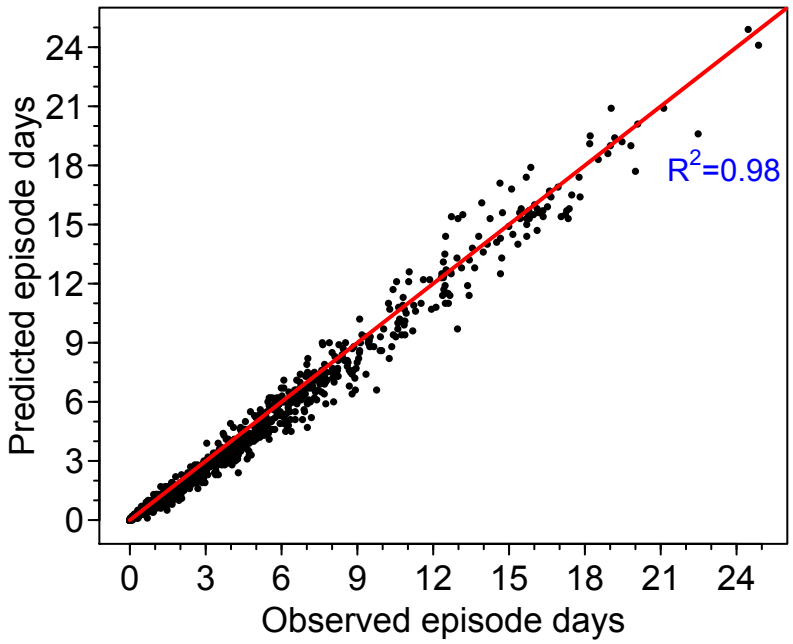

Figure S5. Comparison of observed and simulated ozone episode days in the cross validation across the United States over the 2003-2012 timeframe. For the model evaluation, we use a 10-fold cross-validation, in which we use observations in one year as the test data and the rest as the training data and repeat this process for every year. Each point represents the mean ozone episode days at each site. The red line denotes the 1:1 line. Ozone episode days are defined as days with MDA8 ozone above 75 ppbv.

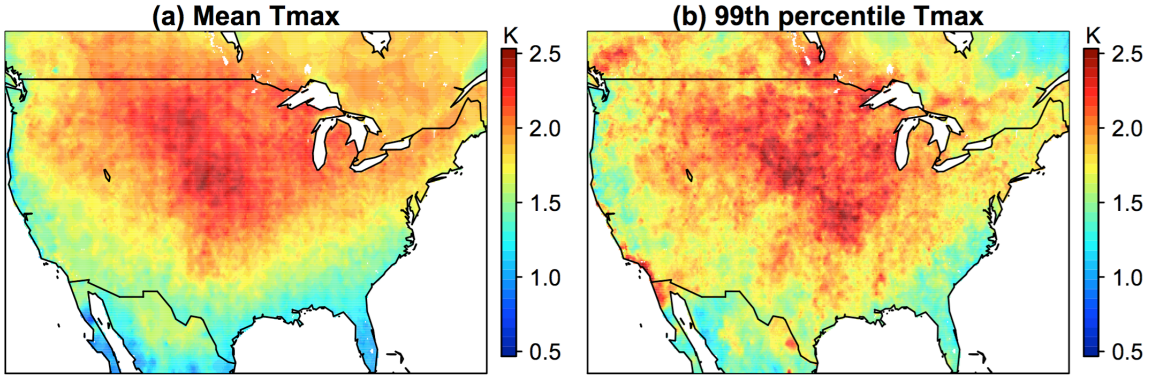

Figure S6. Changes in May-September (a) mean and (b) the 99th percentile daily maximum temperatures (Tmax) from 2000-2009 to 2050-2059 in 19 statistically downscaled CMIP5 climate projections following the RCP4.5 scenario.

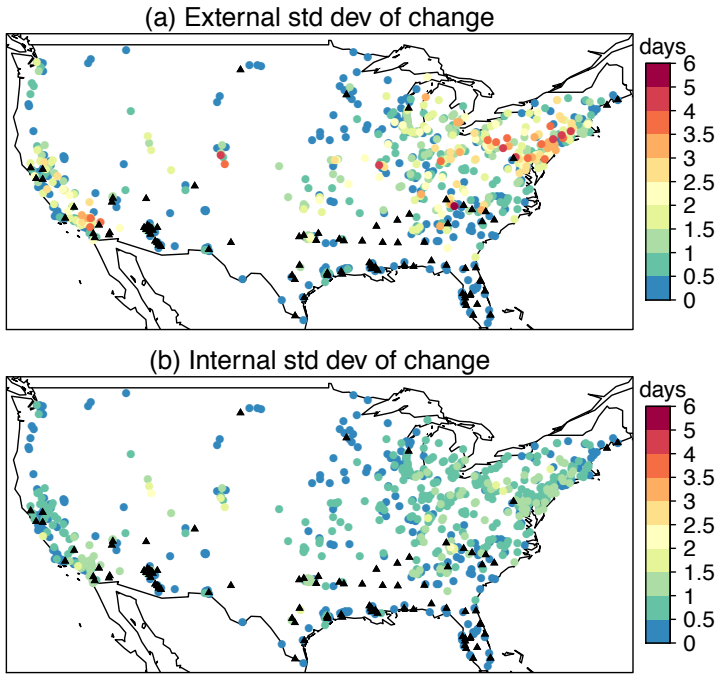

Figure S7. The (a) external and (b) internal standard deviation (std dev) of the simulated changes in ozone episode days across the 19 CMIP5 models at each EPA-AQS site. The external standard deviation refers to the uncertainty caused by the range of temperature projections from the 19 models (E14), while the internal standard deviation refers to the uncertainty in the parameter estimations of the hybrid-EVT model (E13).

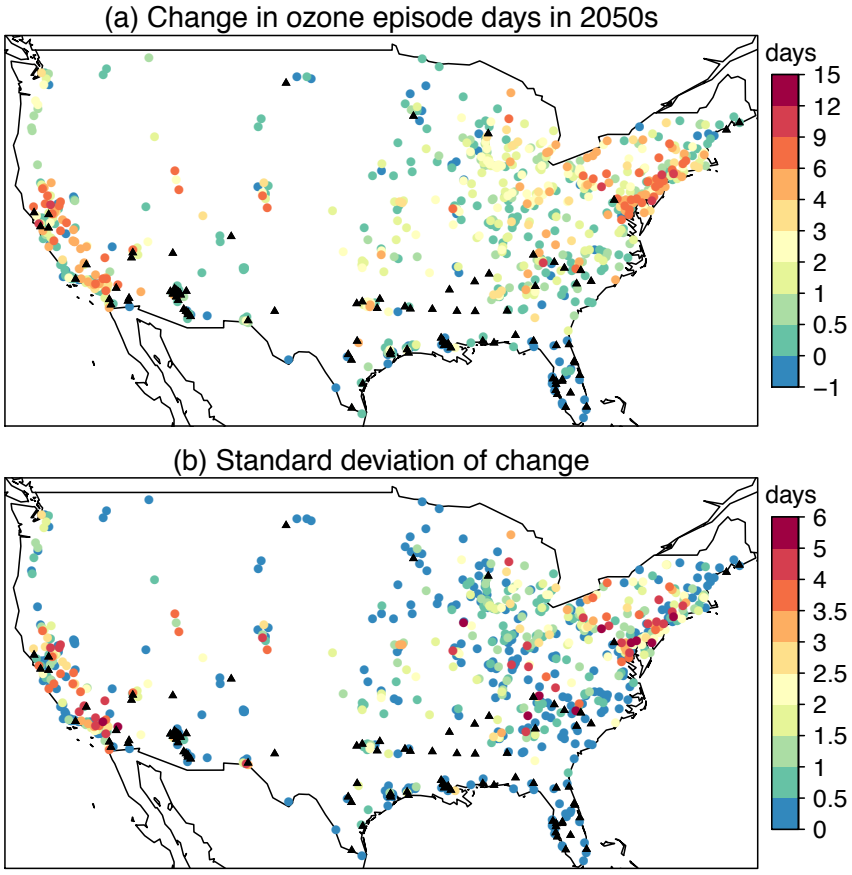

Figure S8. (a) Mean changes from 2000-2009 to 2050-2059 in ozone episode days due to climate change in the RCP4.5 scenario, as calculated using projections of daily mean temperatures (and not maximum temperatures) from 19 CMIP5 models. (b) The standard deviation of the changes in ozone episode days across the 19 CMIP5 models at each site.

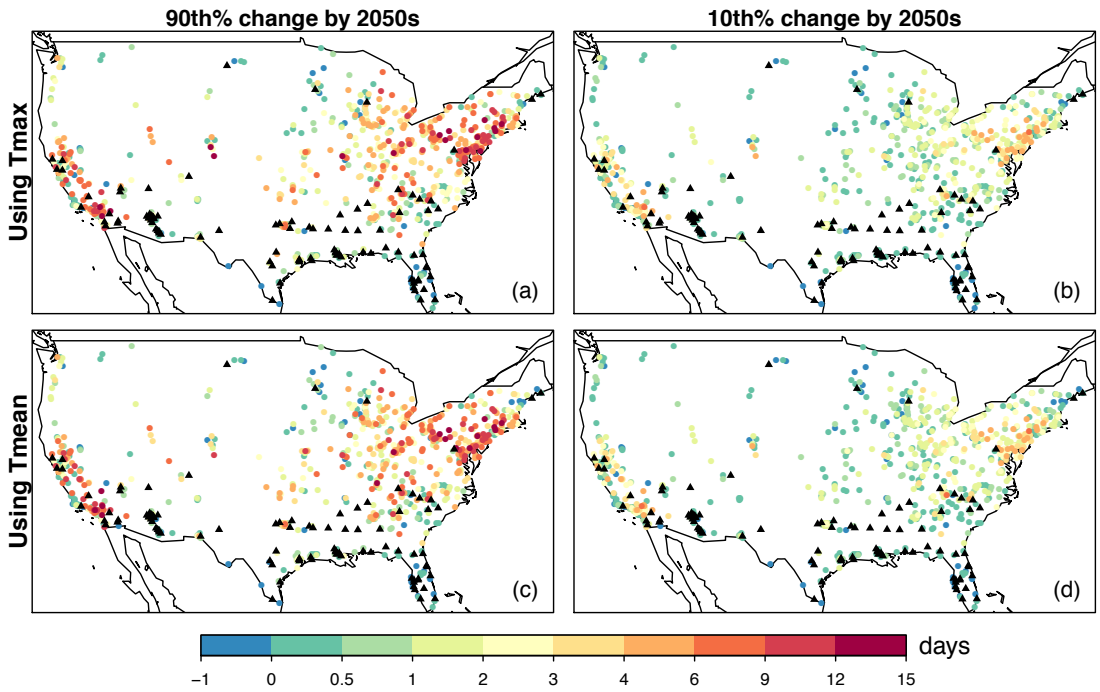

Figure S9. Projected changes in ozone episode days in the (a,c) 90th percentile and (b,d) 10th percentile ranges, as calculated from an ensemble of 19 CMIP5 models. Changes are from 2000-2009 to 2050-2059 due solely to climate change in the RCP4.5 scenario, and are calculated using (a, b) statistically downscaled daily maximum temperatures and (c, d) daily mean temperatures (not downscaled).

Table S1. Models from the Coupled Model Intercomparison Project Phase 5 (CMIP5) used for this study.

Model Name	Institution
ACCESS1-0	Commonwealth Scientific and Industrial Research,Organization (CSIRO) and Bureau of Meteorology (BOM), Australia
BCC-CSM1-1	Beijing Climate Center, China Meteorological Administration
CANESM2	Canadian Centre for Climate Modelling and Analysis
CCSM4	National Center for Atmospheric Research
CESM1-BGC	Community Earth System Model Contributors
CNRM-CM5	Centre National de Recherches Météorologiques / Centre Européen de Recherche et Formation Avancée en Calcul Scientifique
CSIRO-MK3-6-0	Commonwealth Scientific and Industrial Research Organization in collaboration with Queensland Climate Change Centre of Excellence
GFDL-ESM2G	NOAA Geophysical Fluid Dynamics Laboratory
GFDL-ESM2M	NOAA Geophysical Fluid Dynamics Laboratory
INMCM4	Institute for Numerical Mathematics
IPSL-CM5A-LR	Max-Planck-Institut für Meteorologie (Max Planck Institute for Meteorology)
IPSL-CM5A-MR	Max-Planck-Institut für Meteorologie (Max Planck Institute for Meteorology)
MIROC-ESM	Japan Agency for Marine-Earth Science and Technology, Atmosphere and Ocean Research Institute (The University of Tokyo), and National Institute for Environmental Studies
MIROC-ESM-CHEM	Japan Agency for Marine-Earth Science and Technology, Atmosphere and Ocean Research Institute (The University of Tokyo), and National Institute for Environmental Studies
MIROC5	Atmosphere and Ocean Research Institute (The University of Tokyo), National Institute for Environmental Studies, and Japan Agency for Marine-Earth Science and Technology
MPI-ESM-LR	Max-Planck-Institut für Meteorologie (Max Planck Institute for Meteorology)
MPI-ESM-MR	Max-Planck-Institut für Meteorologie (Max Planck Institute for Meteorology)
MRI-CGCM3	Meteorological Research Institute
NORESM1-M	Norwegian Climate Centre

References.

Anderson, D. C., C. P. Loughner, G. Diskin, A. Weinheimer, T. P. Canty, R. J. Salawitch, H. M. Worden, A. Fried, T. Mikoviny, A. Wisthaler, and R. R. Dickerson (2014), Measured and modeled CO and NOy in DISCOVER-AQ: An evaluation of emissions and chemistry over the eastern US, Atmos. Environ., 96, 78-87.

Canty, T. P., L. Hembeck, T. P. Vinciguerra, D. C. Anderson, D. L. Goldberg, S. F. Carpenter, D. J. Allen, C. P. Loughner, R. J. Salawitch, and R. R. Dickerson (2015), Ozone and NOx chemistry in the eastern US: evaluation of CMAQ/CB05 with satellite (OMI) data, Atmos. Chem. Phys., 15, 10965-10982, doi:10.5194/acp-15-10965-2015.

Coles, S. G. (2001), An Introduction to Statistical Modeling of Extreme Values, Springer, New York.

Gilleland, E., and R. W. Katz (2011), New software to analyze how extremes change over time, Eos Trans. AGU, 92(2), 13–14.

Goldberg, D. L., C. P. Loughner, M. Tzortziou, J. W. Stehr, K. E. Pickering, L. T. Marufu, and R. R. Dickerson (2014), Higher surface ozone concentrations over the Chesapeake Bay than over the adjacent land: observations and models from the DISCOVER-AQ and CBODAQ campaigns, Atmos. Environ., 84, 9–19.

Gudmundsson, L., J. B. Bremnes, J. E. Haugen, and T. Engen-Skaugen (2012), Technical Note: Downscaling RCM precipitation to the station scale using statistical transformations—A comparison of methods, Hydrol. Earth Syst. Sci., 16, 3383–3390, doi:10.5194/hess-16-3383-2012.

Guenther, A., X. Jiang, C. L. Heald, T. Sakulyanontvittaya, T. Duhl, L. K. Emmons, and X. Wang (2012), The Model of Emissions of Gases and Aerosols from Nature version 2.1 (MEGAN2.1): An extended and updated framework for modeling biogenic emissions, Geosci. Model Dev., 5(6),1471–1492, doi:10.5194/Gmd-5-1471-2012.

Hudman, R. C., N. E. Moore, A. K. Mebust, R. V. Martin, A. R. Russell, L. C. Valin, and R. C. Cohen(2012), Steps towards a mechanistic model of global soil nitric oxide emissions: implementation and space based-constraints, Atmos. Chem. Phys., 12(16), 7779–7795.

Mao, J., F. Paulot, D. J. Jacob, R. C. Cohen, J. D. Crounse, P. O. Wennberg, C. A. Keller, R. C. Hudman, M. P. Barkley, and L. W. Horowitz (2013), Ozone and organic nitrates over the eastern United States: Sensitivity to isoprene chemistry, J. Geophys. Res. Atmos., 118, 11,256–11,268, doi:10.1002/jgrd.50817.

Maurer, E. P., A. W. Wood,J. C. Adam, D. P. Lettenmaier, and B. Nijssen (2002), A long-term hydrologically-based data set of land surface fluxes and states for the conterminous United States, J. Clim., 15,3237–3251.

Murray, L. T., D. J. Jacob, J. A. Logan, R. C. Hudman, and W. J. Koshak (2012), Optimized regional and interannual variability of lightning in a global chemical transport model constrained by LIS/OTD satellite data, J. Geophys. Res., 117, D20307, doi:10.1029/2012JD017934.

Paulot, F., J. D. Crounse, H. G. Kjaergaard, J. H. Kroll, J. H. Seinfeld, and P. O. Wennberg (2009a), Isoprene photooxidation: New insights into the production of acids and organic nitrates, Atmos. Chem. Phys., 9,1479–1501.

Paulot, F., et al. (2009b),Unexpected epoxide formation in the gas-phase photooxidation of isoprene, Science, 325,730–733, doi:10.1126/science.1172910.

Reiss, R.-D., and M. Thomas (2007), Statistical Analysis of Extreme Values: with applications to insurance, finance, hydrology and other fields, Birkhäuser Basel, 530pp., 3rd edition.

Rieder, H. E., J. Staehelin, J. A. Maeder, T. Peter, M. Ribatet, A. C. Davison, R. Stübi, P. Weihs, and F. Holawe (2010), Extreme events in total ozone over Arosa – Part 1:

Application of extreme value theory,Atmos. Chem. Phys., 10, 10,021–10,031, doi:10.5194/acp-10-10021-2010.

Steiner, A. L., A. J. Davis, S. Sillman, R. C. Owen, A. M. Michalak, and A. M. Fiore(2010), Observed suppression of ozone formation at extremely high temperatures due to chemical and biophysical feedbacks, Proceedings of the National Academy of Sciences, doi:10.1073/pnas.1008336107.

Travis, K., Jacob, et al. (2015), Declining NOx in the Southeast US and implications for ozone-NOx -VOC chemistry, presented at the SEAC4RS Science Team Meeting, 28 April–1 May, Pasadena, Calif.

Yu, S., R. Mathur, J. Pleim,G. Pouliot, D. Wong, B. Eder, K. Schere, R. Gilliam, and S. T. Rao (2012),Comparative evaluation of the impact of WRF/NMM and WRF/ARW meteorology on CMAQ simulations for PM2.5 and its related precursors during the 2006 TexAQS/GoMACCS study,Atmos. Chem. Phys., 12(9),4091–4106, doi:10.5194/acp-12-4091-2012.

Zhang, L., D. J. Jacob, X. Yue, N. V. Downey, D. A. Wood, and D. Blewitt (2014), Sources contributing to background surface ozone in the US Intermountain West, Atmos. Chem. Phys., 14, 5295-5309, doi:10.5194/acp-14-5295-2014.